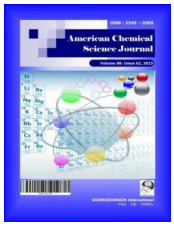

American Chemical Science Journal
14(2): 1-12, 2016, Article no.ACSJ.25366
ISSN: 2249-0205

SCIENCEDOMAIN *international*
www.sciencedomain.org

Removal of Antimony (V) from Aqueous Solution by Iron-based Adsorbents

Yongchao Li[1*], Fei Zhang[1], Xiaoxian Hu[1] and Bozhi Ren[1]

[1]School of Civil Engineering, Hunan University of Science and Technology, China.

Authors' contributions

This work was carried out in collaboration between all authors. Author YL designed the study and wrote the first draft of the manuscript. Authors FZ and XH wrote the protocol, performed the experiments. Author BR managed the analyses of the study. All authors read and approved the final manuscript.

Article Information

DOI: 10.9734/ACSJ/2016/25366
Editor(s):
(1) Pradip K. Bhowmik, Department of Chemistry, University of Nevada Las Vegas, Maryland Parkway, Las Vegas NV, USA.
(2) Francisco Marquez-Linares, Full Professor of Chemistry, Nanomaterials Research Group, School of Science and Technology, University of Turabo, USA.
Reviewers:
(1) S. K. Mendon, The University of Southern Mississippi, USA.
(2) Oupa Ntwampe, University of North West, South Africa.
Complete Peer review History: http://sciencedomain.org/review-history/14378

Original Research Article

Received 29th February 2016
Accepted 23rd April 2016
Published 28th April 2016

ABSTRACT

Antimony pollution has attracted increasing attention for its toxicity. In this study, iron oxide, copper oxide and Fe-Cu binary oxide were synthesized by chemical precipitation/co-precipitation method and investigated using XRD, SEM and FTIR characterizations. Then Sb(V) removal from water by different adsorbents was evaluated. Moreover, the effect of solution pH and initial adsorbents dose was systematically investigated. It was found that removal capacity of kaolinite, aluminum oxide and MWCNTs was poor. However, Sb(V) adsorption on iron oxide and copper oxide was rapid and followed a pseudo-second-order rate law. The equilibrium adsorption capacity increased with the increasing of adsorbent dosage. Especially, when pH <5.0, the removal percentage of Sb(V) by iron oxide sharply increased. Sb(V) uptake by Fe-Cu binary oxide was better than both iron oxide and copper oxide. FTIR analysis confirmed the presence of active -OH and dynamic analysis indicated that chemical adsorption was dominant mechanism for Sb(V) adsorption. Above all, the production process of iron-based adsorbents was simple and they possessed high adsorption ability for Sb(V), Therefore, iron oxide and Fe-Cu binary oxide were promising adsorbents for antimony removal from contaminated water.

**Corresponding author: E-mail: nkliyongchao@163.com;*

Keywords: Sb(V); adsorption; Iron oxide; copper oxide; Fe-Cu binary oxide.

1. INTRODUCTION

Antimony (Sb) is metalloid, and belongs to group VA of the periodic table. It is extensively used in alloys, batteries, flame retardants and power transmission equipment [1]. The environmental behavior of antimony is often similar to that of arsenic [2]. Antimony and its compounds are considered to be hazardous to human health or even carcinogenic [3]. Generally, the trivalent and pentavalent inorganic forms of antimony are the most common species in water solution, and Sb(III) species are known to be 10 times more toxic than Sb(V) species [4]. According to thermodynamic predictions, Sb(V) present in aerobic condition and Sb(III) persisted in anoxic media. However, because of biological activity and kinetic effects, Sb(III) and Sb(V) species frequently coexists in natural waters [5]. Antimony is classified as priority pollutant by the Environmental Protection Agency of the United States [6] and by the European Union [7]. Also, China established 5 $\mu g \cdot L^{-1}$ for antimony as quality standards for surface water in 2002 [8].

Most of the world's environmentally significant antimony pollution is largely due to mining industry which produces a great quantity of antimony mine drainage and antimony waste residue [9]. In China, the antimony mine drainage contains high concentrations of suspended solids, dissolved antimony, arsenic, lead and sulfates etc. Even after precipitation treatment in factories, the typical concentrations of dissolved antimony still ranged from a few $\mu g \cdot L^{-1}$ to a few $mg \cdot L^{-1}$ [10,11]. Now, waters and soils around the mine area were seriously contaminated in China, and the health of plants, aquatic species and humans was endangered [12].

Precipitation [13], coagulation/flocculation [14], electrochemical [15] and adsorption [16] methods have been used for the removal of antimony from aqueous solution. Among these methods, adsorption method is one of the most effective choices for the removal of heavy metal ions from aqueous solutions because of its low cost, simplicity, rapidness and high efficiency. Considering large amounts of antimony mine drainage produced with high level of antimony and sulfate, the context of application is especially important. Significant research has been conducted on antimony adsorption by different kind of materials, such as granular activated carbon, bentonite, multiwall carbon nanotubes, and natural biomaterials [17-20]. Experiments showed Sb(III) removal ability of $FeCl_3$-modified granular-activated carbon was 2.7 mg/g [17]. Sb(III) and Sb(V) removal ability of bentonite was 0.56 and 0.50 mg/g, respectively [18]. The MWCNTs had an adsorption capacity of 0.325 mg Sb(III)/g MWCNTs at pH 7.0 and 298 K [19]. The maximum Sb(III) sorption capacity of *Physcia tribacia* was 81.1 mg/g [20]. Recently, iron and iron oxide were widely used to remove antimony from water. For example, Sb(III) and Sb(V) removal from water by nanoscale zero-valent iron stabilized with polyvinyl alcohol was evaluated. Its maximum adsorption capacity for Sb(III) and Sb(V) was 6.99 and 1.65 $mg \cdot g^{-1}$, respectively [21]. Hematite coated magnetic nanoparticle was fabricated through heterogeneous nucleation technique and used to remove trace Sb(III) from water [22]. Fe-Zr binary oxide adsorbent had a removal capacity of 51 $mg \cdot g^{-1}$ for Sb(V) at pH 7.0 [23]. At pH 5.0, the maximum removal capacity of Sb(V) by Fe-Mn binary oxide, ferric hydroxide and manganese dioxide was 1.05, 0.82 and 0.43 $mmol \cdot g^{-1}$, respectively [24]. Chemical methods are well known and widely accepted methods for bulk production of iron oxide. And chemical co-precipitation method is a widely applicable method for synthesis of binary oxide [25]. There have been relatively investigations addressing the property and mechanism of arsenic binding to different metal oxide adsorbents, and the result was well [26]. However, studies about Sb(V) adsorption capability exerted by different adsorbents were limited, especially metal oxide and bimetal composites. Recently, it was reported that cupric oxide was an effective sorbent for both As(V) and As(III) removal. Although antimony has some similar chemical properties with arsenic, it has seldom been studied for antimony removal.

The objectives of this study were to (1) prepare iron oxide, copper oxide and Fe-Cu binary oxide; (2) compare the relative affinity of Sb(V) for different kinds of adsorbents, including iron powder, nanoscale zero-valent iron, iron oxide and copper oxide; (3) study the effect of adsorbent dose and solution pH on Sb(V) removal. Meanwhile, scanning electron microscopy, Fourier transform infrared spectra, X-ray diffraction and dynamic analysis were used to illustrate the adsorption mechanism.

2. EXPERIMENTAL SECTION

2.1 Chemical Reagents

Deionized water was produced from a Dilli-Q water purification system. It was used to prepare stock solutions and synthetic water. Prior to use, all polyethylene bottles, glassware and sample vessels were immersed in 15% HNO_3 solution, and rinsed with deionized water.

Iron powder was purchased from Tianjin Kemiou Chemical Reagent Co. Ltd., China. Kaolinite and aluminium chloride anhydrous ($AlCl_3$) was obtained from Tianjin Damao Chemical Reagent Factory, China. Iron chloride hexahydrate ($FeCl_3 \cdot 6H_2O$) was purchased from Xilong Chemical Co. Ltd., Guangzhou, China. Cupric sulfate ($CuSO_4$) and sodium hydroxide (NaOH) were purchased from Tianjin Yongda Chemical Reagent Co. Ltd, China. Multiwall carbon nanotubes (MWCNTs) and nanoscale zero-valent iron (NZVI) were purchased from Beijing Boyugaoke New Material Technology Co. Ltd., China, and they were used as received. Potassium pyroantimonate ($KSb(OH)_6$) was from Aladdin Industrial Corporation, Shanghai, China. All the chemicals and reagents used were analytical grade or higher. The Sb(V)-stock solution with an antimony concentration of 100 $mg \cdot L^{-1}$ was prepared by dissolving $KSb(OH)_6$ into 2 $mol \cdot L^{-1}$ HCl solution.

2.2 Preparation and Characterization of Adsorption Materials

Fe-Cu binary oxide with a Fe/Cu molar ratio of 2/1 was prepared by chemical co-precipitation method then treated by drying treatment. The schematic flowchart for the preparation steps of the Fe-Cu binary oxide is illustrated in Fig. 1. Iron oxide was prepared at room temperature (23°C) according to the following procedure: 0.617 $mol \cdot L^{-1}$ $FeCl_3$ was dissolved in 20 mL of deionized water. Then 1.25 $mol \cdot L^{-1}$ NaOH was slowly added into the $FeCl_3$ solution with continuously magnetic stirring until the solution pH was kept in the range of 9–10. After addition, the formed suspension was continuously stirred for 2 h, and then the suspension from centrifuge was washed with deionized water three times. The supernatant was discarded each time after the centrifugal separation. The final product was dried at 80°C for 24 h. The copper oxide and aluminum oxide were synthesized using similar methods. The final dry materials appeared in the form of fine powder.

Particle size and morphology were characterized using scanning electron microscopy (SEM, JSM-6380LV, JEOL, Japan). Chemical composition and crystal structure were examined by and X-ray diffraction (XRD, D8 Advance, Bruker, Germany). For characterization of the functional groups on the surface of prepared adsorbents, Fourier transform infrared (FTIR, Nicolet 6700, USA) spectra of samples were measured by the standard KBr disk method.

2.3 Removal Experiment

Stock solution of 250 mL 100 $mg \cdot L^{-1}$ Sb(V) solution was prepared first. Sb(V) adsorption batch experiment were run in a 125 mL polypropylene bottles containing 100 mL of 20 $mg \cdot L^{-1}$ Sb(V) solution. And the initial solution pH was adjusted to 5.0±0.1 by adding 3 $mol \cdot L^{-1}$ HCl or NaOH. In each test, 0.03 g different adsorbent samples (iron powder, kaolinite, NZVI, iron oxide, aluminum oxide, copper oxide, Fe-Cu binary oxide, MWCNTs) were added to the bottles, respectively. Then, the bottles were shaken on an end-over-end tumbler at 100 rpm for 24 h at 23°C. At timed intervals, samples were taken by a 5 mL-syringe, filtered through 0.45 μm membrane and analyzed for Sb(V) concentrations. Duplicate tests were conducted for all the experiments.

To study the effect of solution pH on Sb(V) adsorption, the initial pH of Sb(V) solution was adjusted to 3.0, 5.0, 7.0 and 9.0 respectively with adding 1.0 $mol \cdot L^{-1}$ HCl or 1.25 $mol \cdot L^{-1}$ NaOH. Then the experiments were carried out by adding 0.03 g NZVI, iron oxide and copper oxide into 100 mL Sb(V) solution respectively. Other conditions were the same as above.

Effect of adsorbents dose on Sb(V) adsorption was investigated at pH 5.0. 0.015, 0.03, and 0.045 g of iron oxide was added to 100 mL 20 $mg \cdot L^{-1}$ Sb(V) solutions, respectively. 0.03, 0.05, and 0.08 g copper oxide was added to 100 mL 20 $mg \cdot L^{-1}$ Sb(V) solutions, respectively. Other conditions were the same as above.

2.4 Analytical Methods

Samples for Sb(V) were analyzed as total antimony by flame atomic absorption spectrophotometer (AA-7001, East & West Analytical Instruments, Inc., Beijing). The detection limit of this method was 0.2 $mg \cdot L^{-1}$, and the analytical regression coefficient R^2 was greater than 0.997. The pH of solution after reaction was measured by a pH meter (PB-10 Sartorius Scientific Instruments Co., Beijing).

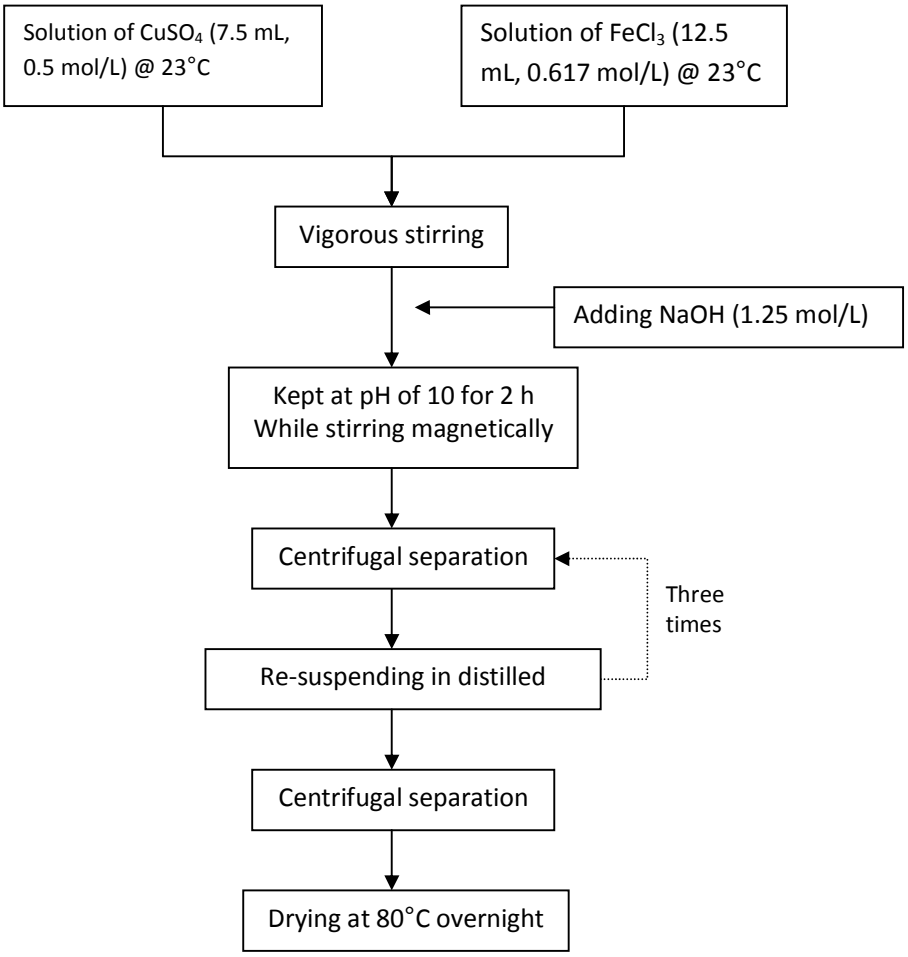

Fig. 1. Flow chart for preparation of Fe-Cu binary oxide using co-precipitation method

3. RESULTS AND DISCUSSION

3.1 Difference in the Fabrication Process of Iron Oxide and Fe-Cu Binary Oxide

Formation of copper oxide and iron oxide was easily discernible due to changes in the color of the solution. Red-brown precipitates were formed by adding NaOH to $FeCl_3$ solution with magnetically stirring. Blue solids were also synthesized by titrating $CuSO_4$ solution to pH 10 with NaOH. Compared with copper oxide, appearance of iron oxide precipitates was more obvious. During the preparation process of Fe-Cu binary oxide with a Fe/Cu molar ratio of 2/1, it was found that the product colour was darker than red-brown, and the blue solid did not occur. Moreover, the prepared Fe-Cu binary oxide settled better than iron oxide in water, which can reduce the loss of Fe^{3+} ion that cannot precipitate completely. As seen in Fig. 2, when Fe-Cu binary oxide settled down, lamination did not appear which indicated that prepared Fe-Cu oxide was not just simple physical mixture of iron oxide and copper oxide.

3.2 SEM Image of Prepared Different Adsorbents

Fig. 3 shows the SEM image of the iron oxide and copper oxide which was synthesized by precipitation method and then dried at 80 °C for 24 h. As shown in Fig. 3a, most of iron oxide particles were massive and compact. They were not of uniform size, certain particles reached the nanometer grade, and some were greater than 10 μm. As can be seen from Fig. 3b, the copper oxide was present as small, acicular particle.

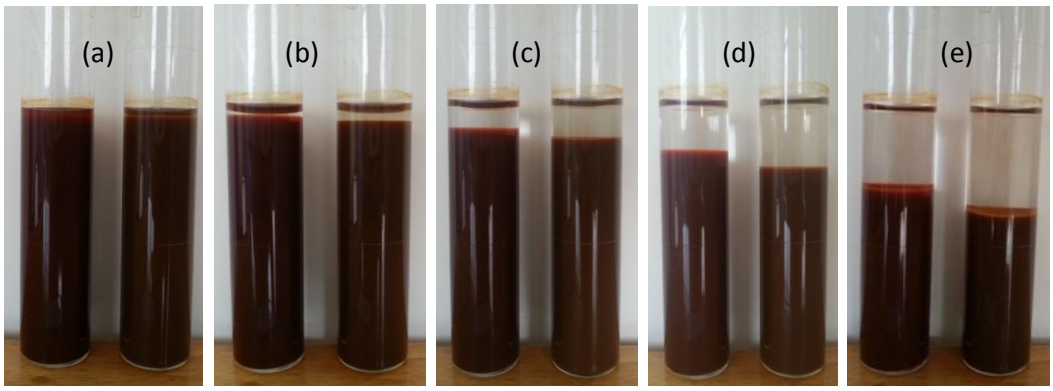

Fig. 2. Tubes containing iron oxide (left) and Fe-Cu binary oxide (right) at various time. (a): after 1 min; (b): after 10 min; (c): after 30 min; (d): after 60 min; (e): after 120 min

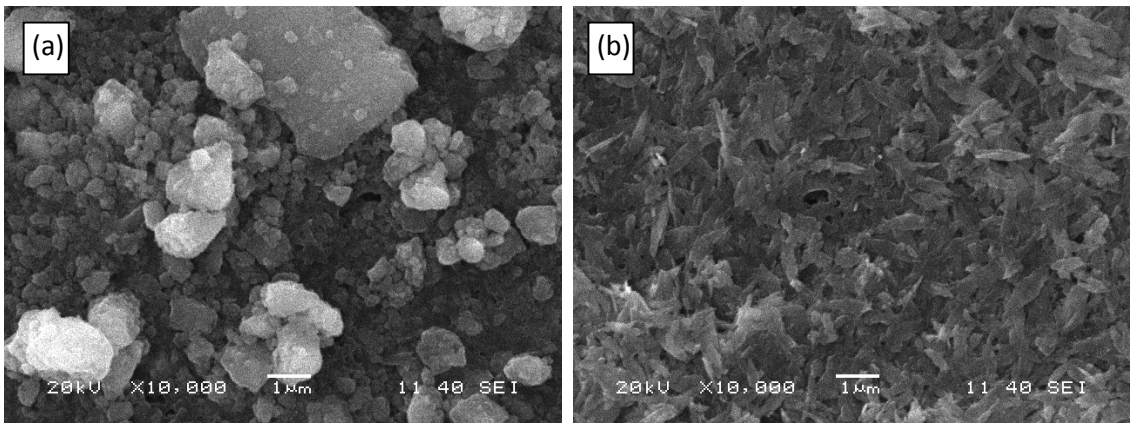

Fig. 3. SEM images of (a) iron oxide and (b) copper oxide

3.3 XRD Pattern of the Adsorbents

Using different preparation methods, the phase composition of iron oxide was also different. Fig. 4 shows phase composition of reaction products that was determined by XRD. Four diffraction peaks observed at 22.3°, 35.34°, 54.2° and 62.52° in Fig. 4a were features of FeOOH [27,28], which was the main iron oxide products. In addition, the presence of broad peaks in X-ray diffraction spectra showed that prepared iron oxide was poorly ordered and amorphous. Fig. 4b shows the XRD patterns of the copper oxide which was effectively prepared via precipitation method using $CuSO_4$. The patterns showed that prepared copper oxide had good crystallinity. The characteristic peaks at 36.2°, 39°, 49.3°and 61.8° were in agreement with those of the standard patterns of CuO [29].

3.4 FTIR Analysis

The FTIR spectra record was carried out in the range of 400-4000 cm^{-1}. Fig. 5 illustrates the FTIR spectra of iron oxide, copper oxide and Fe-Cu binary oxide. The occurrence of band near to 1640 cm^{-1} in all samples was ascribed to the hydroxyl groups of physisorbed water molecules [30]. The peak at 3410 cm^{-1} can be assigned to the stretching vibration of -OH band, which indicated the presence of hydroxyl on these adsorbents [31].

For the iron oxide, the peaks between 1300 cm^{-1} and 1550 cm^{-1} corresponded to the bending vibration of the hydroxyl group associated with Fe. The band at about 500-800 cm^{-1} referred to Fe-O characteristic absorption peaks [32]. However the characteristic peak intensity was not high, and the XRD spectrum also proved that the product was relatively low in crystallinity.

For the copper oxide, the existence of band at 490 cm^{-1} recognized to the vibrations of Cu-O, confirming the formation of copper oxide [33]. Moreover, bands observed at 1005-1170 cm^{-1} were relevant to the asymmetric and symmetric

S-O stretches, which indicated that copper oxide adsorbed some SO_4^{2-} ion. In addition, an approval of cuprous oxide (Cu_2O) peaks at 615 cm^{-1} was detected [34].

For the Fe-Cu binary oxide, two peaks at 1450 and 1350 cm^{-1} were due to the bending vibration of the hydroxyl group associated with Fe and Cu [32]. A new peak at 480 cm^{-1} was different from that of copper oxide and iron oxide, and it may indicate the formation of Fe-Cu binary oxide.

3.5 Comparison of Sb(V) Adsorption on Different Adsorbents

The goal of adsorption experiments at this stage was to provide a preliminary understanding of the adsorption capacity of different adsorbents for Sb(V) ion. Initial Sb(V) concentration of 20 $mg \cdot L^{-1}$ was chosen at their typical concentrations in antimony mine drainage. Fig. 6 shows the reaction data of Sb(V) on different adsorbents as a function of contact time. $[Sb(V)_0]$ and $[Sb(V)]$ denoted the initial and residual concentration after time t, respectively. $\frac{[Sb(V)_0]-[Sb(V)]}{[Sb(V)_0]} \times 100\%$ was used to determine the removal percentage. It can be seen that, Sb(V) removal rate of kaolinite, aluminum oxide, and MWCNTs after 24 h was 2%, 0.5%, and 1.8% respectively. At the same reaction condition, around 19.6%, 45.58%, 66% and 27.7% of Sb(V) was removed by 0.3 $g \cdot L^{-1}$ iron powder, NZVI, iron oxide, copper oxide. It indicated that the removal ability of iron-based adsorbents was optimal. Compared with iron powder, significant adsorption improvement was obtained by NZVI due to increasing specific surface area which provided a large number of adsorption sites. However, nanoscale particles do not show a higher adsorption rate over micro-scale iron oxide and copper oxide. There may be some strong interaction between iron oxide particles and Sb(V), apart from van der Waals attraction. FTIR spectra indicated that iron oxide had large amount of Fe–OH functional groups, which may provide a large number of chemical adsorption sites. Moreover, Xu et al. [24] found $Sb(OH)_6^-$ may form inner-sphere surface complexes at the surface of the Fe-Mn binary oxide. Therefore, the chemical adsorption was the primary reason for the high adsorption ability of iron oxide and copper oxide. Overall, the results showed that iron oxide was significantly more effective at removing Sb(V) than the other adsorbents.

3.6 Effect of pH on Sb(V) Adsorption

Solution pH was one of the more important factors affecting adsorption process, and it was related to speciation of the metal ions in solution and the surface functional groups on the adsorbent. It was known that, positively charged antimony species only occurred in extreme acidic conditions (pH<2). Antimonate ($Sb(OH)_6^-$) was the most common inorganic forms of Sb(V) species present in solution [35]. Furthermore, the pH value of antimony mine drainage was in the range of 3.48-9.88 in China [36]. Therefore, the study of pH effect on Sb(V) adsorption was necessary.

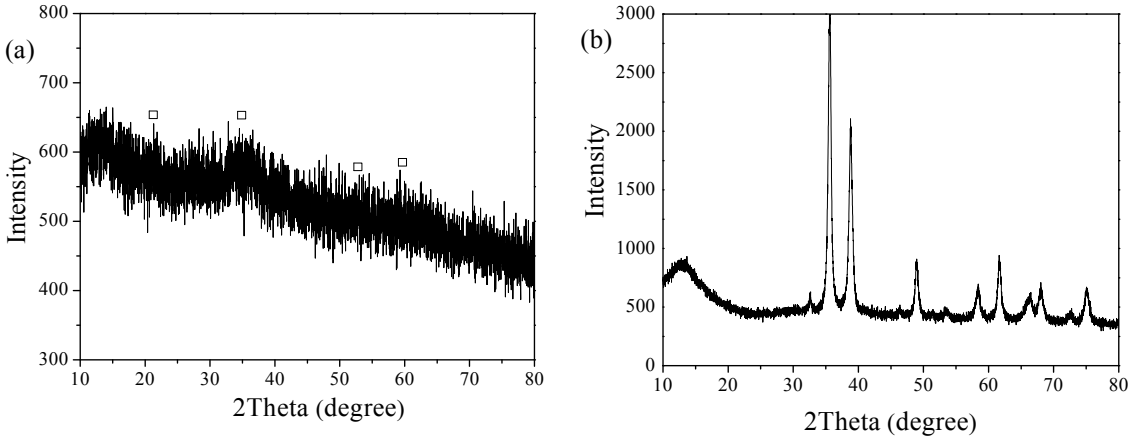

Fig. 4. XRD pattern of prepared (a) iron oxide and (b) copper oxide

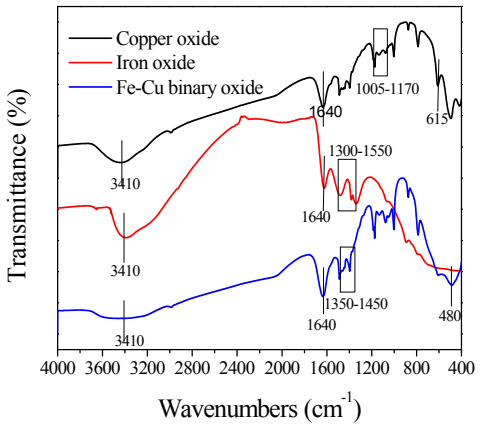

Fig. 5. FTIR spectra of the prepared iron oxide, copper oxide and Fe-Cu binary oxide

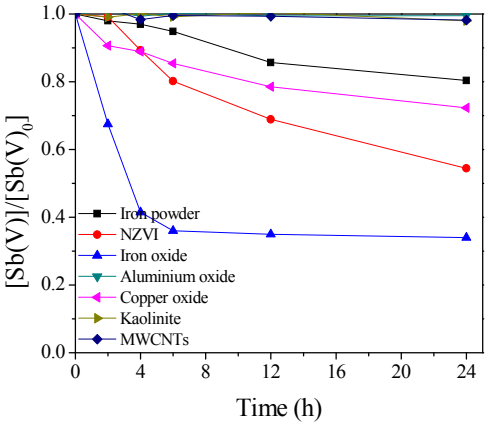

Fig. 6. Removal of 20 mg·L^{-1} Sb(V) by 0.3 g·L^{-1} different adsorbents at initial pH of 5.0

Fig. 7 shows the effect of pH on Sb(V) adsorption on iron oxide, NZVI and copper oxide. It was clear to see that Sb(V) adsorption by iron oxide, NZVI and copper oxide was sensitive to pH variations. For the iron oxide, when the initial solution pH was 3.0, Sb(V) was quickly removed and removal rates reached to 100% after 6.5 h reaction. With the initial solution pH increased to 5.0, 7.0 and 9.0, the removal rate of Sb(V) after 24 h reaction decreased to 69%, 38.1% and 29.6% respectively. After reaction with iron oxide, the pH of Sb(V) solution was changed to 2.92, 6.16, 6.42, 8.15 respectively. When the initial solution pH was 3.0, 5.0, 7.0, 9.0, the removal rate of Sb(V) with copper oxide were 41%, 27.7%, 23.9%, 13.3%, respectively. It was shown that Sb(V) adsorption by copper oxide was not so sensitive as iron oxide to pH variations. Just as iron oxide, the adsorption ability of Sb(V) by NZVI increased with decreasing of initial solution pH. The reason was that in acidic and neutral pH, the surface charge of NZVI and iron oxide was positive because of the protonation reaction. With decreasing pH value, the surface charge was more positive and the electrostatic attraction between the negatively charged $Sb(OH)_6^-$ ion and the positively charged NZVI and iron oxide became stronger, and thereby resulted in the increase of Sb(V) adsorption. Especially, when pH <5.0, the removal percentage of Sb(V) sharply increased.

3.7 Effect of Adsorbent dose on Sb(V) Removal

Unlike acid mine drainage, the acidity of actual antimony mine drainage was not very high, most of which was within a range of weak acids to weak bases [36]. Further the cost of practical application of these nanomaterials can be prohibitive. So, next research was focused on Sb(V) adsorption by iron oxide and copper oxide at initial pH of 5.0.

The influence of adsorbent dose on the Sb(V) removal rates was investigated, and the results are shown in Fig. 8. It shows that increasing the amount of iron oxide and copper oxide resulted in a faster and more extended adsorption of the Sb(V) from water. At an initial iron oxide dose of 0.15, 0.3 and 0.45 g·L^{-1}, about 47.08%, 69% and 89.03% of 20 mg·L^{-1} Sb(V) were removed within 24 h, respectively. At an initial copper oxide dose of 0.3, 0.5 and 0.8 g·L^{-1}, about 27.7%, 44.12% and 77.04% of 20 mg·L^{-1} Sb(V) were removed respectively. In addition, it was observed that the adsorption process of Sb(V) onto these adsorbents could be divided into two steps. In the first step, the adsorption rate was fast and almost 90% of the total adsorption of Sb(V) occurred within the initial 6 h of reaction. The adsorption rate then slowed down significantly.

To elucidate the sorption mechanism, pseudo-first-order and pseudo-second-order kinetics were used to evaluate the dominant mechanism involved in Sb(V) adsorption onto iron oxide and copper oxide. The low value of determination coefficient (R^2) indicated that Sb(V) removal did not follow a pseudo-first-order kinetic. The reaction was described by pseudo-second-order kinetic according to Eq. (1) [37],

$$\frac{t}{q_t} = \frac{1}{k_2 q_e^2} + \frac{t}{q_e} \quad (1)$$

where t (h) is the reaction time, q_e ($mg \cdot g^{-1}$) is and q_t ($mg \cdot g^{-1}$) is the amount of adsorbed Sb(V) at equilibrium and at any time t, k_2 ($g \cdot mg^{-1} \cdot h^{-1}$) is the equilibrium rate constant for pseudo-second-order sorption. The fitted kinetic parameters were shown in Table 1. Obviously, q_e increased with increasing of adsorbent dosage. As being indicated from R^2 values in Fig. 9, the pseudo-second-order model was suitable to describe the adsorption of Sb(V) onto iron oxide and copper oxide. This just showed the dominant mechanism of chemisorptions involved. Again the appearance of massive active hydroxyl group supported for this view.

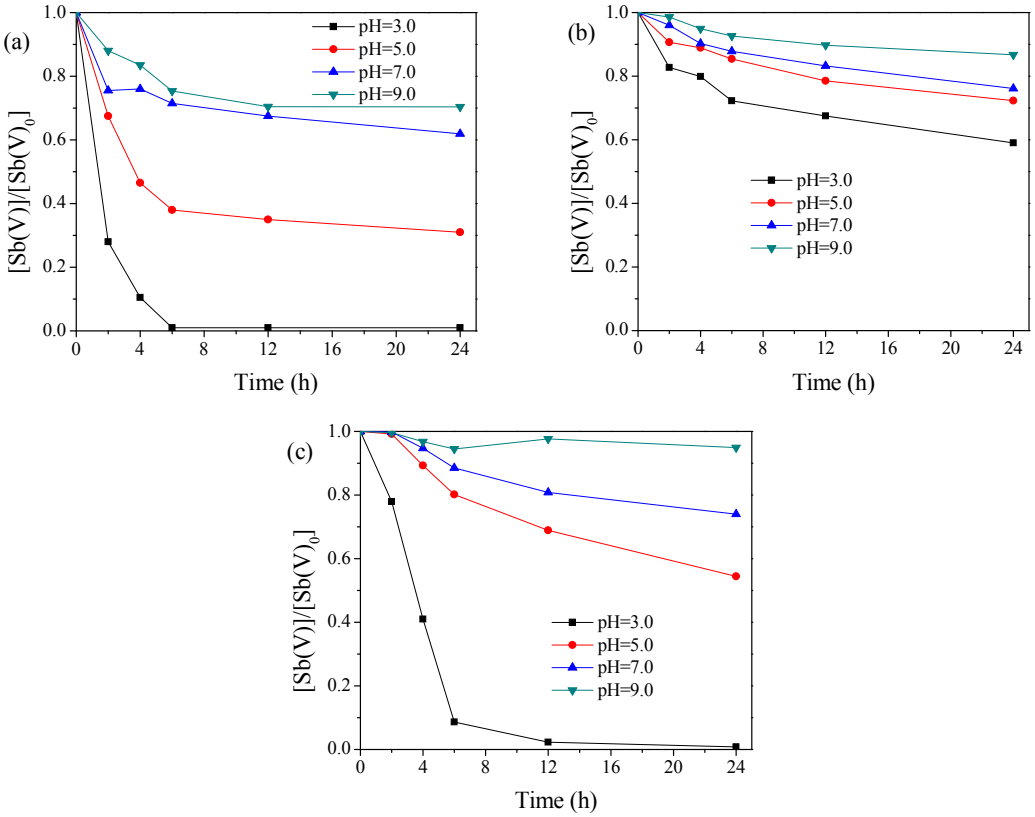

Fig. 7. Effect of pH on Sb(V) removal for (a) iron oxide; (b) copper oxide; (c) NZVI. Initial adsorbent dose was 0.3 $g \cdot L^{-1}$ and Sb(V) concentration was 20 $mg \cdot L^{-1}$ in all cases

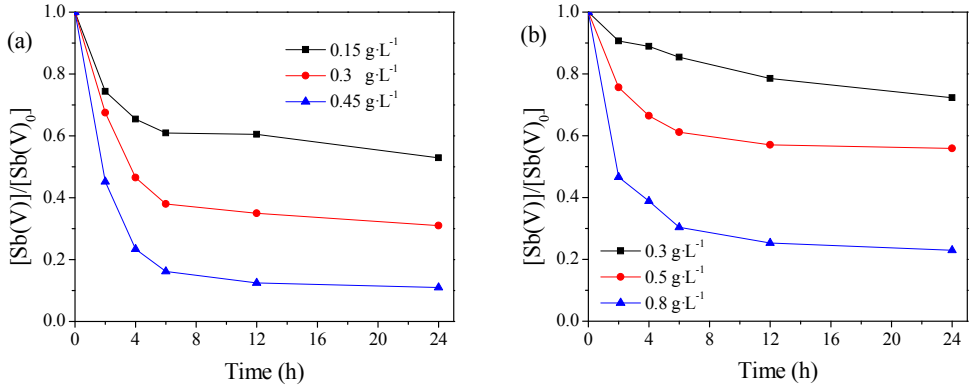

Fig. 8. Effect of adsorbent dose on Sb(V) removal from solution for (a) iron oxide and (b) copper oxide. Initial Sb(V) concentrations was 20 $mg \cdot L^{-1}$, and pH was 5.0

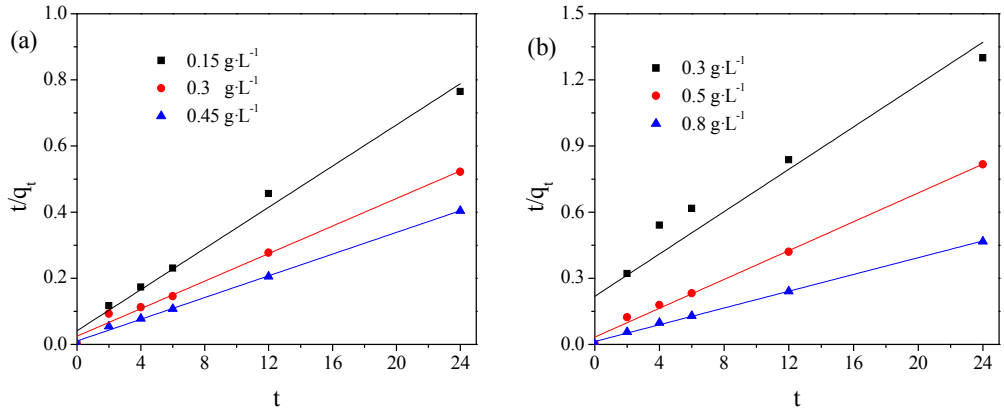

Fig. 9. Kinetics of Sb(V) removal by (a) iron oxide and (b) copper oxide with different dose. Initial Sb(V) concentrations was 20 mg·L^{-1}, and pH was 5.0

3.8 A Preliminary Study of Sb(V) Removal with Fe-Cu Binary Oxide

Fig. 10a highlights the variation of the adsorbed Sb on Fe-Cu binary oxide with a Fe/Cu molar ratio of 2/1. Fig. 10b shows that Sb(V) removal by Fe-Cu binary oxide followed a pseudo-second-order kinetic. It was calculated that q_e was approximately 58.89 mg·g^{-1} and k_2 was 0.03844 g·mg^{-1}·h^{-1}. However, at the same reaction condition, q_e was 48.08 and 20.82 mg·g^{-1} and k_2 was 0.017516 and 0.010578 g·mg^{-1}·h^{-1} for iron oxide and copper oxide, respectively. It was obvious that the adsorption rate and uptake of Sb(V) ions by obtained Fe-Cu binary oxide at equilibrium were higher than both iron oxide and copper oxide. Moreover, it can reduce the loss of Fe^{3+} ion with adding Cu^{2+} ion in water solution during Fe-Cu binary oxide preparation. In brief, simple process of preparing and high removal capacity in this study revealed that Fe-Cu binary oxide could be a better adsorbent for the removal of Sb(V) from antimony mine drainage. In addition, this material outperformed many other reported adsorbents for Sb(V), such as nano-zero valent iron stabilized by polyvinyl alcohol [21], Fe-Zr bimetal oxide [23], goethite [38], and so on. Although the maximum adsorption capacity of Fe-Cu binary oxide was lower than that of Fe-Mn binary oxide (127.89 mg·g^{-1}, pH 5.0), the initial Sb(V) concentration was as high as 60 mg·L^{-1} in research of Xu et al. [24], that could put on the calculated removal ability.

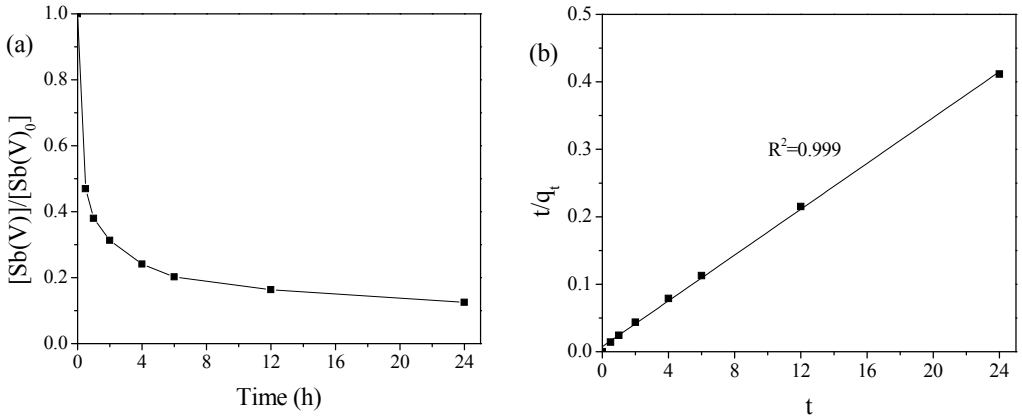

Fig. 10. (a) Performance and (b) kinetic of Sb(V) removal by Fe-Cu binary oxide at pH of 5.0. Initial Fe-Cu binary oxide dose was 0.3 g·L^{-1}, and Sb(V) concentrations was 20 mg·L^{-1}

Table 1. Kinetics constants for Sb(V) adsorption on the iron oxide and copper oxide

Pseudo-second-order model							
Iron oxide				Copper oxide			
Dose ($g \cdot L^{-1}$)	k_2 ($g \cdot mg^{-1} \cdot h^{-1}$)	q_e ($mg \cdot g^{-1}$)	R^2	Dose ($g \cdot L^{-1}$)	k_2 ($g \cdot mg^{-1} \cdot h^{-1}$)	q_e ($mg \cdot g^{-1}$)	R^2
0.15	0.023476	32.15	0.987	0.3	0.010578	20.82	0.894
0.3	0.017516	48.08	0.990	0.5	0.032111	30.58	0.994
0.45	0.025862	60.97	0.997	0.8	0.027348	52.63	0.997

4. CONCLUSIONS

Different kinds of adsorbents were used to remove Sb(V) from water solution. Kaolinite, aluminum oxide and MWCNTs almost had no removal ability for Sb(V). Around 19.6%, 45.58%, 66% and 27.7% of 20 $mg \cdot L^{-1}$ of Sb(V) was removed by 0.3 $g \cdot L^{-1}$ iron powder, NZVI, iron oxide, copper oxide at the same reaction condition. NZVI and iron oxide performed well under acid conditions, especially at pH< 5.0. Kinetic results revealed that Sb(V) sorption onto iron oxide and copper oxide followed a pseudo-second-order kinetic model. Compared with iron oxide and copper oxide, significant adsorption improvement was gained by Fe-Cu binary oxide with a Fe/Cu molar ratio of 2/1 which was successfully prepared through a co-precipitation method. Furthermore, it showed a capacity of 58.89 $mg \cdot g^{-1}$ at pH 5.0 with an initial Sb(V) concentration of 20 $mg \cdot L^{-1}$. The high Sb(V) adsorption ability of the iron-based adsorbent was mainly due to the chemisorption process. However, intensive research was need for Sb(V) adsorption mechanism with iron oxide and Fe-Cu binary oxide.

COMPETING INTERESTS

Authors have declared that no competing interests exist.

REFERENCES

1. Shotyk W, Krachler M, Chen B. Antimony: Global environmental contaminant. Journal of Environmental Monitoring. 2005;7: 1135–1136.
2. Wilson SC, Lockwood PV, Ashley PM, Tighe M. The chemistry and behaviour of antimony in the soil environment with comparisons to arsenic: A critical review. Environmental Pollution. 2010;158:1169–1181.
3. Smichowski P, Madrid Y, Camara C. Analytical methods for antimony speciation in waters at trace and ultratrace levels: A review. Fresenius Journal of Analytical Chemistry. 1998;360:623–629.
4. Sigel HG, Sigel A, Sigel H. Handbook on metals in clinical and analytical chemistry. Marcel Dekker Inc, New York, 1994;227–236.
5. Filella M, Belzile N, Lett MC. Antimony in the environment: A review focused on natural waters. III. Microbiota relevant interactions. Earth-Science Reviews. 2007;80:195–217.
6. United States Environmental Protection Agency, Water related fate of the 129 priority pollutants, Washington DC, USA; 1979.
7. Council of the European Communities, Council Directive 76/464/EEC of 4 May 1976 on pollution caused by certain dangerous substances discharged into the aquatic environment of the community. Official Journal L. 1976;129:23–29.
8. China's EPA. Surface water environmental quality standard, Beijing, China; 2002.
9. Filella M, Williams PA, Belzile N. Antimony in the environment: Knowns and unknowns. Environmental Chemistry. 2009;6:95–105.
10. He MC, Wang XQ, Wu FC, Fu ZY. Antimony pollution in China. Science of the Total Environment. 2012;421:41–50.
11. Huang Y, Hu J, Li JS, Sun L, Chai LY. Emission status survey and control measure discussion on antimony pollutant of antimony industrial. Environmental Science & Technology. 2010;33:252–255. (in Chinese)
12. Wu FC, Fu ZY, Liu BJ, Mo CL, Chen B, Corns W, Liao HQ. Health risk associated with dietary co-exposure to high levels of antimony and arsenic in the world's largest antimony mine area. Science of the Total Environment. 2011;409:3344–3351.
13. Du J. Study on the treatment of antimony ore tailings wastewater. Gansu non-Ferrous Metal. 1995;4:32-35. (in Chinese)
14. Guo XJ, Wu ZJ, He MC. Removal of antimony(V) and antimony(III) from

drinking water by coagulation-flocculation-sedimentation (CFS). Water Research. 2009;43:4327–4335.
15. Henry Bergmann ME, Savas Koparal A. Electrochemical antimony removal from accumulator acid: Results from removal trials in laboratory cells. Journal of Hazardous Materials. 2011;196:59–65.
16. Dorjee P, Dulasiri A, Xing BS. Antimony adsorption by zero-valent iron nanoparticles (nZVI): Ion chromatography-inductively coupled plasma mass spectrometry (IC-ICP-MS) study. Microchemical Journal. 2014;116:15–23.
17. Yu TC, Wang XH, Li C. Removal of antimony by $FeCl_3$-modified granular-activated carbon in aqueous solution. Journal of Environmental Engineering. 2014;140:A4014001.
18. Xi JH, He MC, Lin CY. Adsorption of antimony(III) and antimony(V) on bentonite: Kinetics, thermodynamics and anion competition. Microchemical Journal. 2011; 97:85–91.
19. Salam MA, Mohamed RM. Removal of antimony(III) by multi-walled carbon nanotubes from model solution and environmental samples. Chemical Engineering Research and Design. 2013;91:1352–1360.
20. Uluozlu OD, Sari A, Tuzen M. Biosorption of antimony from aqueous solution by lichen (*Physcia tribacia*) biomass. Chemical Engineering Journal. 2010;163: 382–388.
21. Zhao XQ, Dou XM, Mohan D, Pittman CU, OK YS, Jin X. Antimonate and antimonite adsorption by a polyvinyl alcohol-stabilized granular adsorbent containing nanoscale zero-valent iron. Chemical Engineering Journal. 2014;6:4268–4274.
22. Shan C, Ma ZY, Tong MP, Efficient removal of trace antimony(III) through adsorption by hematite modified magnetic nanoparticles. Journal of Hazardous Materials. 2014;268: 229–236.
23. Li XH, Dou XM, Li JQ. Antimony(V) removal from water by iron-zirconium bimetal oxide: Performance and mechanism. Journal of Environmental Sciences. 2012;24:1197–1203.
24. Xu W, Liu RP, Qiu JH, Peng RM. The adsorption behaviors of Fe-Mn binary oxide towards Sb(V). Acta Scientiae Circumstantiae. 2012;32:270–275. (in Chinese)
25. Dave PN, Chopda LV. Application of iron oxide nanomaterials for the removal of heavy metals. Journal of Nanotechnology. 2014;2014:1-14.
26. Ungureanu G, Santos S, Boaventura R, Botelho C. Arsenic and antimony in water and wastewater: Overview of removal techniques with special reference to latest advances in adsorption. Journal of Environmental Management. 2015;151: 326–342.
27. Jiang W, Lv JT, Luo L, Yang K, Lin YF, Hu FB, Zhang J, Zhang SZ. Arsenate and cadmium co-adsorption and co-precipitation on goethite. Journal of Hazardous Materials. 2013;262:55–63.
28. Yürüm A, Kocabas-Ataklı ZÖ, Sezen M, Semiat R, Yürüm Y. Fast deposition of porous iron oxide on activated carbon by microwave heating and arsenic(V) removal from water. Chemical Engineering Journal. 2014;242:321–332.
29. Habibi MH, Karimi B. Application of impregnation combustion method for fabrication of nanostructure CuO/ZnO composite oxide: XRD, FESEM, DRS and FTIR study. Journal of Industrial and Engineering Chemistry. 2014;20:1566–1570.
30. Zhang GS, Qu JH, Liu HJ, Liu RP, Li GT. Removal mechanism of As(III) by a novel Fe-Mn binary oxide adsorbent: Oxidation and sorption. Environmental Science & Technology. 2012;41:4613–4619.
31. Li YC, Jin ZH, Li TL. A novel and simple method to synthesize SiO_2-coated Fe nanocomposites with enhanced Cr(VI) removal under various experimental conditions. Desalination. 2012;288:118–125.
32. Xu W, Wang HJ, Liu RP, Zhao X, Qu JH. The mechanism of antimony(III) removal and its reactions on the surfaces of Fe–Mn binary oxide. Journal of Colloid and Interface Science. 2011;363:320–326.
33. Sankar R, Manikandan P, Malarvizhi V, Fathima T, Shivashangari KS, Ravikumar V. Green synthesis of colloidal copper oxide nanoparticles using *Carica papaya* and its application in photocatalytic dye degradation. Spectrochimica Acta Part A: Molecular and Biomolecular Spectroscopy. 2014;121:746–750.
34. Liu XQ, Li Z, Zhang Q, Li F. Controllable synthesis and enhanced photocatalytic properties of $Cu_2O/Cu_{31}S_{16}$ composites.

Materials Research Bulletin. 2012;47: 2631–2637.
35. Filella M, Belzile N, Chen YW. Antimony in the environment: A review focused on natural waters. II. Relevant solution chemistry. Earth-Science Reviews. 2002;59:265–285.
36. Zhu J, Wu FC, Deng QJ, Shao SX, Mo CL, Pan XL, Li W, Zhang RY. Environmental characteristics of water near the Xikuangshan antimony mine. Hunan Province. Acta Scientiae Circumstantiae. 2009;29:655–661. (in Chinese)
37. Ho YS, McKay G. Pseudo-second order model for sorption processes. Process Biochemistry. 1999;34:451–465.
38. Leuz AK, Mönch H, Johnson CA. Sorption of Sb(III) and Sb(V) to goethite: Influence on Sb(III) oxidation and mobilization. Environmental Science & Technology. 2006;40:7277–7282.

Peer-review history:
The peer review history for this paper can be accessed here:
http://sciencedomain.org/review-history/14378